

Knowledge-Transfer based Cost-effective Search
for Interface Structures:
A Case Study on fcc-Al [110] Tilt Grain
Boundary

Tomohiro Yonezu¹, Tomoyuki Tamura^{*2,3}, Ichiro Takeuchi^{1,3}, and
Masayuki Karasuyama^{†1,3,4}

¹ Department of Computer Science, Nagoya Institute of
Technology, Gokiso, Showa, Nagoya, Aichi 466-8555, Japan

² Department of Physical Science and Engineering, Nagoya
Institute of Technology, Gokiso, Showa, Nagoya, Aichi 466-8555,
Japan

³ Center for Materials research by Information Integration,
National Institute for Materials Science, Tsukuba 305-0047, Japan

⁴ PRESTO, Japan Science and Technological Agency, 4-1-8
Honcho, Kawaguchi, Saitama, 332-0012, Japan

*Corresponding author tamura.tomoyuki@nitech.ac.jp

†Corresponding author karasuyama@nitech.ac.jp

Abstract

Determining the atomic configuration of an interface is one of the most important issues in the materials research. Although theoretical simulations are effective tools for that purpose, the exhaustive search is computationally prohibitive due to high degrees of freedom of the interface structure. For the fast exploration of the interface structures, we introduce two machine-learning concepts, called transfer learning and cost-sensitive search. To solve multiple different (but related) tasks, transferring knowledge of each task improves efficiency of machine-learning methods. In the interface-structure search, multiple energy surfaces created by a variety of different orientation angles need to be explored to understand interface properties. A knowledge-transfer based machine-learning algorithm can provide an efficient search for the interface structures by exploiting similarity among multiple energy surfaces. Further, we consider diversity of supercell sizes of interface models, which results in a different computational cost of each search space. The idea of the cost-sensitive search is to compare candidate structures based on both of a possible energy decrease and the computational cost, meaning that each candidate is evaluated by its cost-effectiveness for the energy decrease. By combining the above two machine-learning concepts, our method realizes a cost-effective simultaneous search for multiple energy surfaces. As a case study, we show efficiency of our method using the fcc-Al [110] tilt grain boundary.

1 Introduction

A *grain boundary* (GB) is the interface between two grains or crystallines in a polycrystalline material, and has a significantly different atomic configuration from a single crystal. Since this causes peculiar mechanical and electrical properties of materials, one of the most important issues in materials research is determining the atomic configuration of an interface. Experimental observations, such as the atomic-resolution transmission electron microscope (TEM) observation [1], and theoretical simulations, such as first-principles calculations based on density functional theory and static lattice calculations with empirical potentials, have been extensively performed to investigate interface structures.

Determining an interface structure by using theoretical simulations needs huge computational cost due to the geometrical degree of freedom. Nine degrees of freedom are present in a GB: five macroscopic and four microscopic [2], and huge number of GB models should be considered. In even a simplified coincidence site lattice (CSL) GB, namely a Σ GB, for a monoatomic system, three dimensional *rigid body translation* (RBT) states should be considered. To understand the whole nature of GBs, one has to obtain stable interface structures over all rotation angles and all rotation axes. In a straightforward manner, all possible candidates of GB models are optimized and the lowest-energy configuration is obtained. But this approach is practically exhausting, and developing efficient approaches to determining the interface structure without searching all possible candidates is strongly demanded.

In recent years, materials informatics techniques based on *machine learning* have been introduced in the literature as an inexpensive means of exploiting materials data [3]. For the structure search, which is our main interest in this paper, a machine learning technique called *Bayesian optimization* [4] has proven its usefulness mainly by the application to determining stable bulk structures [5, 6]. Bayesian optimization is a general global optimization method which is based on a Bayesian inference of the search space, and it can deal with a variety of material-discovery problems, such as identifying the low energy region in

a potential energy surface [7]. For the interface structure, some papers [8, 9] proposed to apply Bayesian optimization to the GB-structure search, and shown its efficiency, for example, by using the fcc-Cu $\Sigma 5$ [001](210) CSL GB. However, their search method is a standard Bayesian optimization same as the method employed in the bulk case, and the search methodology specific for GBs has not been introduced so far to the best of our knowledge.

We consider a general problem setting in the GB-structure search which is to explore a variety of rotation angles for some fixed rotation axis. Suppose that we have T different angles to search, and candidate structures are created by RBTs for each of them. A naive approach to this problem is to apply some search method, such as Bayesian optimization [8, 9], T times separately, but this approach is not efficient because it ignores the following two important characteristics of the GB structure:

1. Energy-surface similarity: The energy surfaces of different angles are often quite similar. This similarity is explained by *structural unit model* [10, 11, 12, 13] which has been widely accepted to describe GB structures in many materials. This model suggests that different GBs can contain common structural units, and then they share the similar local atomic environments. Although structurally similar GBs can produce similar energy surfaces, the naive approach does not utilize this similarity and restarts the structure search from scratch for each angle.
2. Cost imbalance: The computational time scales as $O(M) \sim O(M^3)$ for number of atoms M in the supercells, depending on the computational scheme. GB supercells usually have a variety of sizes because of the diversity of the Σ value, which is the inverse density of lattice sites. This means that computational costs for large Σ GBs dramatically increase because the number of atoms in a supercell increases. Thus, the structure search for large Σ GBs is more time-consuming than small Σ GBs.

Figure 1 shows (a) calculated stable GB energies for fcc-Al [110] tilt GBs and (b) energy surfaces created by two dimensional RBTs for the rotation angles 141°

(top), 134° (bottom left) and 145° (bottom right). The entire landscape of the surfaces are similar, while their computational costs are largely different since the biggest supercell ($\Sigma 89$) contains almost 10 times larger number of atoms than the smallest supercell ($\Sigma 9$).

In this paper, we propose a machine-learning based stable structure search method which is particularly efficient for GB by taking two characteristics of the GB-structure into account. For energy-surface similarity, we introduce a machine-learning concept called *transfer learning* [14]. The basic idea is to transfer knowledge among different (but related) tasks to improve efficiency of machine-learning methods. A *task* is a GB-structure search for a fixed angle in this paper. When tasks have similarity each other, information accumulated for one specific task can be useful for the other tasks. For our structure-search problem, in a perspective of the Bayesian inference, a sampled GB model for an angle provides information to other angles probabilistically, given some similarity measure between angles. A variety of similarity measures are available to describe angle differences, including the rotation angle and radial distribution of atoms, and thus we can exploit similarity among structure searches with different angles for fast convergence of the optimization. For the cost imbalance issue, we introduce a *cost-sensitive* search. Our method incorporates cost information into the sampling decision, which means that we evaluate each candidate based on both of a possibility of an energy improvement and a cost of sampling. By combining the cost-sensitive search with transfer learning, our method accumulates information by sampling low cost surfaces in the initial stage of the search, and can identify the stable structures in high cost surfaces with a small number of sampling based on transferred surface information. As a case study, we evaluate cost-effectiveness of our method based on fcc-Al [110] tilt GBs.

2 Methods

2.1 Problem Setting

Suppose that we have $t = 1, \dots, T$ different rotation angles θ_t , for each of which we have N_t candidate-GB models created by *rigid body translations* (RBTs). Figure 2 shows an example of a supercell of a $\Sigma 9$ GB model (see § 3.1 for detail of our GB model), from which N_t GB models are created by RBTs. The total number of the GB models is denoted as $N = \sum_{t=1}^T N_t$. We would like to search the stable GB structures with respect to *all* of the given rotation angles. In this paper, GB energy is defined against the total energy of the bulk crystal as

$$E_{\text{GB}} = \frac{E_{\text{GB}}^{\text{tot}} - E_{\text{bulk}}}{2S}, \quad (1)$$

where E_{GB} is the total energy of the GB supercell, E_{BS} is the bulk energy with the same number of atoms as the GB supercell, and S is the cross-section area of the GB model in the supercell. In the denominator, the cross-section area S is multiplied by 2 since the supercell contains two GB planes as shown in Figure 2. Note that the GB energy for each GB model is calculated through *atomic relaxation*. A set of GB energies for all N GB models is represented as a vector $\mathbf{E} = (E_{\text{GB}}^{(1)}, \dots, E_{\text{GB}}^{(N)})^\top$, where $E_{\text{GB}}^{(i)}$ is the GB energy of the i -th GB model.

A stable structure search for some fixed angle can be mathematically formulated as a problem to find lower energy structures with a smaller number of “sampling” from candidates. The number of candidate structures is often too large to exhaustively compute their energies, and we usually do not know the exact energy surface as a function in the search space. This problem setting is thus sometime called *black-box optimization problem* in the optimization literature. We call a stable structure search for each angle a “task”.

Let $\tau_i \in \{1, \dots, T\}$ be the task index that the i -th GB model is included, and C_t be a cost to compute the GB energy in the t -th task. We assume that the cost can be easily estimated based on the employed computational method and the number of atoms in the supercell. For example, *embedded atom method*

(EAM) [15] needs $O(M)$ computations, where M is the number of atoms in a supercell. Then, we can set C_t as the number of atoms M in a supercell. Instead of counting the number of sampling, we are interested in the sum of the cost C_t taken in the search process, for more practical evaluation of search efficiency. Assuming that a set $\mathcal{S} \subseteq \{1, \dots, N\}$ is an index set of sampled GB models, the total cost of sampling is written as

$$C = \sum_{i \in \mathcal{S}} C_{\tau_i}. \quad (2)$$

2.2 Single-task Bayesian Optimization

Bayesian optimization is a machine-learning method for solving general black-box optimization, and it has been shown to be effective for materials-search problems [5, 6, 7, 8, 9]. The basic idea is to estimate a stable structure iteratively, based on a probabilistic model which is statistically constructed by using already sampled structures. Here, we briefly review a basic concept and technical details of Bayesian optimization for some fixed t -th angle, which we call single-task Bayesian optimization (STB) in this paper.

Gaussian process regression (GPR) [16] is a probabilistic model which is often employed in Bayesian optimization. GPR represents *uncertainty* of unobserved energies by using a random variable vector with a multivariate Gaussian distribution:

$$\mathbf{f} \sim \mathcal{N}(\mathbf{u}, \mathbf{K}), \quad (3)$$

where $\mathbf{f} = (f_1, \dots, f_{N_t})^\top$ is a vector of random variables for approximating the energies \mathbf{E} , and $\mathcal{N}(\mathbf{u}, \mathbf{K})$ is a Gaussian distribution having $\mathbf{u} \in \mathbb{R}^{N_t}$ as a mean vector and $\mathbf{K} \in \mathbb{R}^{N_t \times N_t}$ as a covariance matrix. Note that since we here only focus on the search for a fixed angle θ_t , the indexes of GB models are $1, \dots, N_t$. Let $\mathbf{x}_i \in \mathbb{R}^p$ be a p dimensional descriptor vector for the i -th GB model. The i, j -th element of the covariance matrix is defined by a *kernel function* $k(\mathbf{x}_i, \mathbf{x}_j)$ which gives similarity of two arbitrary GB models i and j . As a kernel function

$k : \mathbb{R}^p \times \mathbb{R}^p \rightarrow \mathbb{R}$, the following Gaussian kernel is often employed:

$$k(\mathbf{x}_i, \mathbf{x}_j) = \exp(-\gamma \|\mathbf{x}_i - \mathbf{x}_j\|_2^2), \quad (4)$$

where $\gamma > 0$ is a scaling parameter and $\|\cdot\|_2$ is the L_2 norm.

When we already have GB energies for a subset of GB models $\mathcal{S} \subseteq \{1, \dots, N_t\}$, GPR updates its predictions for unknown GB energies using a conditional probability. Let $\mathbf{v}_{\mathcal{S}}$ be a sub-vector of an arbitrary vector $\mathbf{v} \in \mathbb{R}^{N_t}$ with the elements corresponding to \mathcal{S} , and $\mathbf{M}_{\mathcal{S}}$ be a sub-matrix of an arbitrary matrix $\mathbf{M} \in \mathbb{R}^{N_t \times N_t}$ with the rows and the columns corresponding to \mathcal{S} . The conditional probability, called *predictive distribution*, of the i -th GB model given energies for \mathcal{S} is written as

$$f_i | \mathbf{E}_{\mathcal{S}} \sim \mathcal{N}(\mu(\mathbf{x}_i), \sigma(\mathbf{x}_i)), \quad (5)$$

where $f_i | \mathbf{E}_{\mathcal{S}}$ is a random variable f_i after observing $\mathbf{E}_{\mathcal{S}}$, and

$$\mu(\mathbf{x}_i) = \mathbf{K}_{i,\mathcal{S}} (\mathbf{K}_{\mathcal{S}} + \epsilon \mathbf{I})^{-1} (\mathbf{E}_{\mathcal{S}} - \mathbf{u}_{\mathcal{S}}), \quad (6)$$

$$\sigma(\mathbf{x}_i) = k(\mathbf{x}_i, \mathbf{x}_i) - \mathbf{K}_{i,\mathcal{S}} (\mathbf{K}_{\mathcal{S}} + \epsilon \mathbf{I})^{-1} \mathbf{K}_{\mathcal{S},i}, \quad (7)$$

in which $\mathbf{K}_{i,\mathcal{S}}$ is a row vector having the i -th row and the columns of \mathcal{S} in \mathbf{K} (and $\mathbf{K}_{\mathcal{S},i}$ is its transpose), and $\epsilon \geq 0$ is a noise term.

In Bayesian optimization, a function called *acquisition function* evaluates a possibility that each candidate GB model would be more stable than the sampled GB models in \mathcal{S} . *Expected improvement* (EI) is one of most standard acquisition functions to select a next structure:

$$\text{EI}_i = \mathbb{E}_{f_i | \mathbf{E}_{\mathcal{S}}} (\max\{0, E^{\text{best}} - f_i\}), \text{ for } i = 1, \dots, N_t, \quad (8)$$

where $\mathbb{E}_{f_i | \mathbf{E}_{\mathcal{S}}}$ is an expectation with respect to $f_i | \mathbf{E}_{\mathcal{S}}$, and E^{best} is the minimum energy among already computed GB models \mathcal{S} . EI is an expected value (based on the predictive distribution of the current GPR) of the energy decrease. Bayesian optimization iteratively selects a next GB model by taking the maximum of EI, and the newly computed GB model is added to \mathcal{S} .

2.3 Multi-task Bayesian Optimization

Although energy surfaces for different angles are often quite similar, STB can not utilize the surface similarity and searches each surface independently. In machine learning, it has been known that, for solving a set of similar tasks, transferring (or sharing) the knowledge (or data) across the tasks can be effective. This idea is called *transfer learning* [14]. In our problem setting, we have multiple structure search tasks for which efficiency of the search can be improved by transferring knowledge of the surfaces. We here introduce a technique called *multi-task learning*, which is a standard transfer-learning method. Bayesian optimization with multi-task learning is called multi-task Bayesian optimization (MTB) in this paper.

To transfer knowledge among different tasks, we employ *multi-task Gaussian process regression* (MTGPR) [17]. Let $\mathbf{z}_t \in \mathbb{R}^q$ be a *descriptor of the t -th task*, and $k^{(\text{task})} : \mathbb{R}^q \times \mathbb{R}^q \rightarrow \mathbb{R}$ be a kernel function for a given pair of tasks. For example, a rotation angle can be a task descriptor (See § 3.2 for our setting of the task descriptors). The task kernel function $k^{(\text{task})}(\mathbf{z}_t, \mathbf{z}_{t'})$ provides similarity of two given tasks t and t' . We employ the following form of the kernel function to define $k^{(\text{task})}$:

$$k^{(\text{task})}(\mathbf{z}_t, \mathbf{z}_{t'}) = \alpha \exp\left(-\gamma^{(\text{task})} \|\mathbf{z}_t - \mathbf{z}_{t'}\|_2^2\right) + (1 - \alpha)\delta_{t,t'} \quad (9)$$

where $\gamma^{(\text{task})} > 0$ and $\alpha \in [0, 1]$ are parameters, and $\delta_{t,t'}$ is defined as 1 if $t = t'$ otherwise 0. The additional parameter α is to control independence of tasks. When we set $\alpha = 1$, $k^{(\text{task})}(\mathbf{z}_t, \mathbf{z}_{t'})$ is 1 only when $t = t'$, and 0 for all other cases. This special case is reduced to apply T separated Gaussian process models for all tasks independently.

MTGPR is defined by a kernel constructed as a product of two kernels on \mathbf{x} and \mathbf{z} . The i, j -element of the covariance matrix of MTGPR is defined as

$$\mathbf{K}_{i,j}^{(\text{MT})} = k(\mathbf{x}_i, \mathbf{x}_j)k^{(\text{task})}(\mathbf{z}_{\tau_i}, \mathbf{z}_{\tau_j}), \text{ for } i, j = 1, \dots, N. \quad (10)$$

Note that we here use the index $1, \dots, N$ across all T tasks, and the task in which the i -th GB model is contained is represented as $\tau_i \in \{1, \dots, T\}$. Then,

we define random variables for unobserved energies by

$$\mathbf{f} \sim \mathcal{N}(\mathbf{u}, \mathbf{K}^{(\text{MT})}), \quad (11)$$

where $\mathbf{f} = (f_1, \dots, f_N)^\top$ is the random variable vector for GB energy and $\mathbf{u} \in \mathbb{R}^N$ is a mean vector. Given a set of already sampled GB models is $\mathcal{S} \in \{1, \dots, N\}$, the predictive distribution is derived by the same manner as in GPR:

$$f_i | \mathbf{E}_{\mathcal{S}} \sim \mathcal{N}(\mu^{(\text{MT})}(\mathbf{x}_i), \sigma^{(\text{MT})}(\mathbf{x})), \quad (12)$$

where

$$\mu^{(\text{MT})}(\mathbf{x}_i) = \mathbf{K}_{i,\mathcal{S}}^{(\text{MT})} \left(\mathbf{K}_{\mathcal{S}}^{(\text{MT})} + \epsilon \mathbf{I} \right)^{-1} (\mathbf{E}_{\mathcal{S}} - \mathbf{u}_{\mathcal{S}}), \quad (13)$$

$$\sigma^{(\text{MT})}(\mathbf{x}_i) = \mathbf{K}_{i,i}^{(\text{MT})} - \mathbf{K}_{i,\mathcal{S}}^{(\text{MT})} \left(\mathbf{K}_{\mathcal{S}}^{(\text{MT})} + \epsilon \mathbf{I} \right)^{-1} \mathbf{K}_{\mathcal{S},i}^{(\text{MT})}. \quad (14)$$

Figure 3 is a schematic illustration of MTGPR. In addition to the structure descriptor \mathbf{x} , the axis of the task descriptor \mathbf{z} is introduced in the figure. The knowledge of the surface is transferred through this axis based on the similarity evaluated by the task kernel. The figure also shows that the accuracy of the function estimation is improved by the transfer (b), compared to the single-task estimation (c).

2.4 Cost-sensitive Acquisition Function

For the cost-imbalance issue, we introduce a *cost-sensitive* acquisition function. In the cost-sensitive acquisition function, to select a next candidate to compute, each GB model is evaluated based not only on the possible improvement of the energy but also on the computational cost of that GB model. This strategy prefers low cost GB models in the early phase of the search, and explores high cost GB models after the information of the energy surface is accumulated. This enables us to identify stable GB structures with a smaller number of samplings in the high cost energy surfaces than methods which ignore cost differences. MTB with the cost-sensitive acquisition function is denoted as CMTB (cost-sensitive MTB).

For the cost-sensitive selection of a next GB model, we use the following acquisition function:

$$\text{EI}_i^{(\text{CMTB})} = \frac{\mathbb{E}_{f_i|\mathcal{E}_S}(\max\{0, E_{\tau_i}^{\text{best}} - f_i\})}{C_{\tau_i}}, \quad (15)$$

where E_t^{best} is the current minimum energy (included in \mathcal{S}) for the t -th task. This acquisition function selects the best GB model to sample in a sense of the expected improvement of the GB energy *per* computational cost, while usual EI without the cost consideration selects a structure in a sense of the expected improvement of the GB energy per sampling iteration. This means that $\text{EI}_i^{(\text{CMTB})}$ is effective to minimize the GB energy while keeping the total cost in Eq. (2) as small as possible.

Figure 4 shows a schematic illustration of CMTB. In the figure, the two surfaces are low cost to sample and the other two surfaces are high cost. CMTB first selects low cost surfaces and accumulates surface information, by which the minimums in high cost surfaces can be efficiently identified.

3 Results (Case Study on fcc-Al)

In this section, we demonstrate effectiveness of the proposed method through stable GB-structure searches for fcc-Al [110] tilt GBs.

3.1 GB Model

We first constructed fcc-Al [110] symmetric tilt (ST) GBs using the coincidence site lattice (CSL) model. The CSL is usually characterized by the Σ value, which is defined as the reciprocal of the density of the coincident sites. Figure 2 (a) shows an example of a supercell of a $\Sigma 9$ STGB model. Two symmetric GBs are introduced to satisfy three-dimensional periodicity. To avoid artificial interactions between GBs, we set the distances between GBs more than 10 Å. For an atomic pair nearer than the cut-off, one of the two is removed if the calculated GB energy (Calculation method is described later.) with the removal of one atom is smaller than that without the removal. For the energy calculations and atomic relaxations, we used the EAM potential for Al in Ref. [15], and the computational time scales as $O(M)$ for the number of atoms M with the linked-list cell algorithm. Figure 2 (b) shows the construction of a supercell by RBT from the STGB model. Figure 5 shows the number of atoms M for all 31 angles. We see that GB models contain largely different numbers of atoms in the supercells from 34 to 370 which results in strong cost imbalance in the search space. For each angle, the two-dimensional RBTs, denoted as X and Y which are illustrated in Figure 2 (b), were generated (we omit the other axis, i.e., Z axis, which did not have strong effect on the energy surface in this time). The grid space is 0.02Å for the direction X , and 0.01Å for the direction Y . In total, we created 17188 candidate GB models for which the exhaustive search is computationally expensive.

3.2 Settings of Gaussian Process

As the descriptor for each GB model \mathbf{x} , we employed the two-dimensional axes of RBTs: X and Y . The kernel function for \mathbf{x} was the Gaussian kernel with the parameter γ set by median heuristics (γ is set as the reciprocal of median of the squared distances). For the task descriptor \mathbf{z} , we used rotation angle θ and radial distribution function (RDF) of the $(X, Y) = (0, 0)$ GB model. As an angle descriptor, we applied the following transformation to the rotation angles: $\tilde{\theta}_t = \theta_t$ if $\theta_t \leq 90$, otherwise $\tilde{\theta}_t = 180 - \theta_t$. In the case of the fcc-Al [100] GBs, θ_t and $\tilde{\theta}_t$ is equivalent. Although the complete equivalence does not hold for fcc-Al [110] GBs, we used this transformed angle as an approximated similarity measure. We defined the task kernel as

$$k^{(\text{task})}(\mathbf{z}_t, \mathbf{z}_{t'}) = \alpha \exp\left(-\gamma_{\theta}^{(\text{task})} \|\tilde{\theta}_t - \tilde{\theta}_{t'}\|_2^2 - \gamma_{\text{RDF}}^{(\text{task})} \|\boldsymbol{\rho}_t - \boldsymbol{\rho}_{t'}\|_2^2\right) + (1 - \alpha)\delta_{t,t'}$$

where $\boldsymbol{\rho} \in \mathbb{R}^{100}$ is a vector created from RDF by taking 100 equally spaced grids from 0 to 6 Å. In this case, the task descriptor is written as $\mathbf{z}_t = (\tilde{\theta}_t, \boldsymbol{\rho}_t^\top)^\top$, and the kernel evaluates the task similarity based on both of the angle and RDF. In other words, two tasks which have similar angles and RDFs simultaneously are regarded as similar in MTGP. The parameters $\gamma_{\theta}^{(\text{task})}$ and $\gamma_{\text{RDF}}^{(\text{task})}$ was set by median heuristics again, and the independency parameter α is estimated by *marginal likelihood maximization* [16]. For each task, the values of the mean parameter \mathbf{u} was set separately as the average of sampled GB energies. The noise term parameter ϵ was also selected by marginal likelihood maximization. The parameter tuning for α and ϵ was performed every 10 samplings. Cost parameter C_t was set by the number of atoms in each supercell.

3.3 Performance Evaluation

We compared the following five methods:

1. random sampling (Random): At each iteration, a next candidate was randomly selected with uniform sampling.

2. single task Bayesian optimization (STB): STB is the conventional Bayesian optimization described in § 2.2. At each iteration, a GB model which had the maximum EI was selected across all the angles.
3. cost-sensitive single task Bayesian optimization (CSTB): CSTB is same as STB except that EI is divided by the cost C_t .
4. multi-task Bayesian optimization (MTB): MTB is Bayesian optimization with multi-task GP by which surface knowledge of different angles is transferred each other. For the acquisition function, we here employed usual EI.
5. cost-sensitive multi-task Bayesian optimization (CMTB): CMTB is MTB with the cost-sensitive acquisition function.

All methods started with randomly selected one structure in each angle, and the results are shown as an average with 10 trials with different initial sampling.

Figure 6 shows a performance comparison. We refer to the difference between the lowest energy identified by some method and the true minimum as a energy gap. The vertical axis of the figure is the average of the gaps for the 31 different angles, and the horizontal axis is the total cost (2). We first focus on the difference between the single-task based methods and the multi-task based methods. The decrease of the single-task based methods (STB and CSTB) are much slower than multi-task based methods (MTB and CMTB). Until about $C = 25000$, the random selection is even comparable with the single-task based methods. In general, Bayesian optimization increases its accuracy with the increase of sampled data, and the multi-task based methods can fully exploit sampled data since MTGP shares the data across different tasks (angles). For the effect of the cost-sensitive acquisition function, we see that both of single-task and multi-task based methods improved their convergence. However, we here note that the cost-sensitive approach is beneficial especially for multi-task methods since it can transfer knowledge accumulated in low cost surfaces to high cost surfaces, while single-task methods does not transfer the

surface information. We will see the effect of the cost-sensitive acquisition function in more detail (in Figure 9). The sum of the computational costs for all candidate structures is $\sum_{i=1}^N C_{\tau_i} = 2993914$. The ratios of the computational cost that CMTB needed to reach 10 mJ/m², 5 mJ/m² and 1 mJ/m² average energy gap were $0.0048 \approx 14363.4/2993914$, $0.0060 \approx 17975.8/2993914$ and $0.0108 \approx 32214.6/2993914$, respectively.

Figures 7 and 8 are angle-wise comparisons of GB energies, and distances between the true minimums and identified GB structures, respectively. The both figures are averages of the 10 runs for random, STB (conventional Bayesian optimization), and CMTB. In Figure 7, all the energies are normalized in such a way that the minimum for each angle becomes zero. We see that the energies identified by CMTB were much closer to the true minimums particularly for $C = 20000$ and $C = 30000$, while STB did not show clear advantage even compared to the random selection. In CMTB, the task $t = 19$ has the relatively large GB energy compared to the other tasks at $C = 20000$ and 30000 . This task corresponds to the $\Sigma 81$ GB model containing 308 atoms in the supercell, which is one of the highest cost surfaces. To observe the search progress in more detail, Figure 8 compares convergence in the RBT space (X, Y) for each angle. Let $\mathcal{S}_t = \{\tau_i = t \mid i \in \mathcal{S}\}$ be a set of sampled GB models from the t -th task. Suppose that $(X^{(\mathcal{S}_t)}, Y^{(\mathcal{S}_t)})$ is the RBT which has the minimum energy among the sampled GB models \mathcal{S}_t , and $(X^{(O_t)}, Y^{(O_t)})$ is the RBT which has the true minimum for the task t . The vertical axis of Figure 8 is defined by $\sqrt{(X^{(\mathcal{S}_t)} - X^{(O_t)})^2 + (Y^{(\mathcal{S}_t)} - Y^{(O_t)})^2}$ (Note that this distance can increase even when the GB energy decreases). In the plot, we can clearly see that CMTB approached to the minimums much faster than the other two methods. In CMTB, the task $t = 19$, which had the large GB energy in Figure 7, is not particularly large compared to the other several tasks having large distances.

To observe the effect of the cost-sensitive acquisition function (15) on the sampling, Figure 9 compares the search progress of MTB and CMTB. In the figure, the plotted value is taken from the Bayesian optimization iteration at which 3 GB models are sampled from the t -th task, i.e., $|\mathcal{S}_t| = 3$ (note that

the iterations are different for different horizontal axis values). The tasks in the horizontal axis are sorted by the ascending order of C_t . Each vertical axis is defined by a subtraction of a result of MTB from CMTB, and thus the bar plots become negative when CMTB has smaller values than MTB. Figure 9 (a) compares the number of sampled GB models $|\mathcal{S}|$ when $|\mathcal{S}_t| = 3$. We see that CMTB has smaller values for low cost tasks, while larger values for high cost tasks compared to MTB. This indicates that CMTB first accumulated surface information using low cost surfaces before sampling from high cost surfaces. Figure 9 (b) compares the lowest energies identified by CMTB and MTB. Although the energy difference fluctuates (because it depends on many factors including similarity relations among tasks), as a general tendency, we see that CMTB achieved lower energies for high cost surfaces, while MTB has lower energies for low cost surfaces, relatively. This indicates cost-effectiveness of CMTB because reducing sampling from high cost surfaces lead low total cost as indicated by Figure 6

4 Conclusions

We introduced a multi-task Bayesian optimization (MTB) based simultaneous structure search for a variety of rotation angles of grain boundary (GB). Each GB structure search can be regarded as a “task”, and our basic idea is to transfer/share knowledge about the energy surfaces among different tasks. This strategy is effective because GBs having different angles often have quite similar energy surfaces due to their similarity of structural units. Further, we also considered the imbalance of the computational cost of GB models caused by a different sizes of supercells. We employed an acquisition function which incorporates cost information in addition to the expected value of the improvement. By using the fcc-Al [110] tilt GBs, we demonstrated the effectiveness of our method compared to random search and conventional Bayesian optimization.

Acknowledgement

We would like to thank R. Arakawa for helpful discussions on GB models. This work was financially supported by grants from the Japanese Ministry of Education, Culture, Sports, Science and Technology to I.T. (16H06538, 17H00758), M.K. (16H06538, 17H04694), Japan Science and Technology Agency (JST) PRESTO to M.K. (Grant Number JPMJPR15N2), and by “Materials research by Information Integration” Initiative (MI²I) project of Support Program for Starting Up Innovation Hub from JST to T.T., I.T., and M.K..

References

- [1] M. Haider, S. Uhlemann, E. Schwan, H. Rose, B. Kabius, and K. Urban. *Nature*, 392:768–769, 1998.
- [2] A. P. Sutton and R. W. Balluffi. *Interfaces in Crystalline Materials*. Oxford University Press, 1995.
- [3] J. R. Rodgers and D. Cebon. *MRS Bulletin*, 31(12):975980, 2006.
- [4] B. Shahriari, K. Swersky, Z. Wang, R. P. Adams, and N. de Freitas. *Proceedings of the IEEE*, 104(1):148–175, 2016.
- [5] A. Seko, A. Togo, H. Hayashi, K. Tsuda, L. Chaput, and I. Tanaka. *Phys. Rev. Lett.*, 115:205901, Nov 2015.
- [6] T. Ueno, T. D. Rhone, Z. Hou, T. Mizoguchi, and K. Tsuda. COMBO: An efficient bayesian optimization library for materials science. *Materials Discovery*, 4:18 – 21, 2016.
- [7] K. Toyoura, D. Hirano, A. Seko, M. Shiga, A. Kuwabara, M. Karasuyama, K. Shitara, and I. Takeuchi. *Phys. Rev. B*, 93:054112, Feb 2016.
- [8] S. Kiyohara, H. Oda, K. Tsuda, and T. Mizoguchi. *Japanese Journal of Applied Physics*, 55(4):045502, 2016.

- [9] S. Kikuchi, H. Oda, S. Kiyohara, and T. Mizoguchi. *Physica B: Condensed Matter*, 2017.
- [10] A. P. Sutton and V. Vitek. *Philos. Trans. R. Soc.*, 309:1, 1983.
- [11] A. P. Sutton and V. Vitek. *Philos. Trans. R. Soc.*, 309:37, 1983.
- [12] A. P. Sutton and V. Vitek. *Philos. Trans R. Soc.*, 309:55, 1983.
- [13] A. P. Sutton and R. W. Balluff. *Philos. Mag. Lett.*, 61:91, 1990.
- [14] S. J. Pan and Q. Yang. *IEEE Transactions on Knowledge and Data Engineering*, 22(10):1345–1359, 2010.
- [15] Y. Mishin, D. Farkas, M. J. Mehl, and D. A. Papaconstantopoulos. *Phys. Rev. B*, 59:3393, 1999.
- [16] C. E. Rasmussen and C. K. I. Williams. *Gaussian Processes for Machine Learning (Adaptive Computation and Machine Learning)*. The MIT Press, 2005.
- [17] E. Bonilla, K. M. Chai, and C. Williams. In J.C. Platt, D. Koller, Y. Singer, and S. Roweis, editors, *Advances in Neural Information Processing Systems 20*, pages 153–160. MIT Press, Cambridge, MA, 2008.

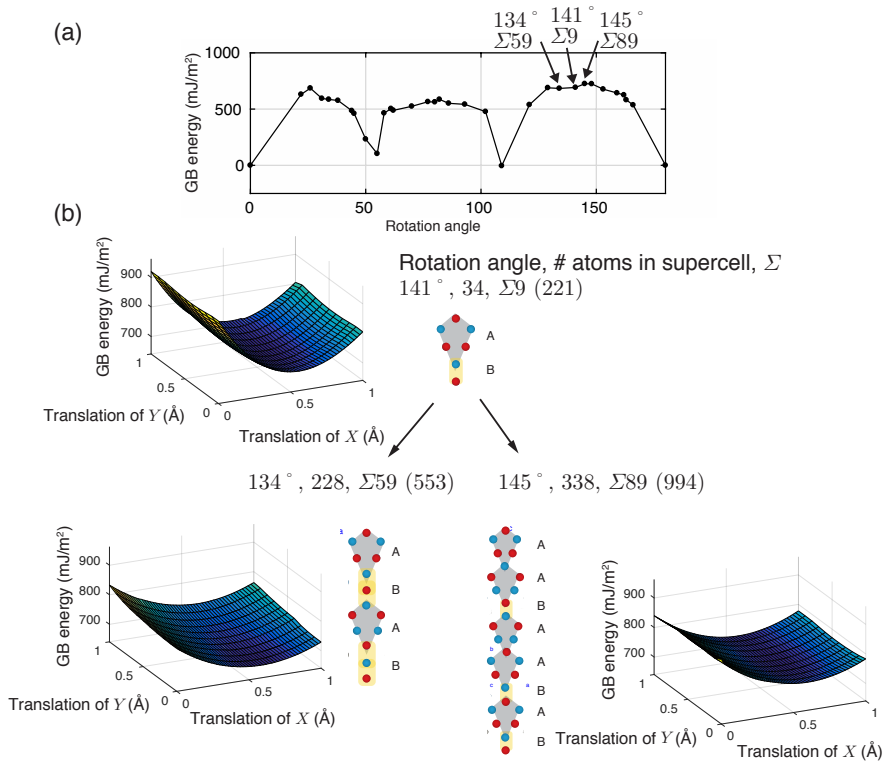


Figure 1: (a) Calculated stable GB energies as a function of the rotation angle for fcc-Al [110] tilt GB, and (b) energy surfaces created by two dimensional RBTs for the angles 141° (top), 134° (bottom left) and 145° (bottom right). The structural units are also shown along with the surfaces in which the units are denoted as A and B. The red and light blue balls denote Al atoms in (110) and (220) atomic layers.

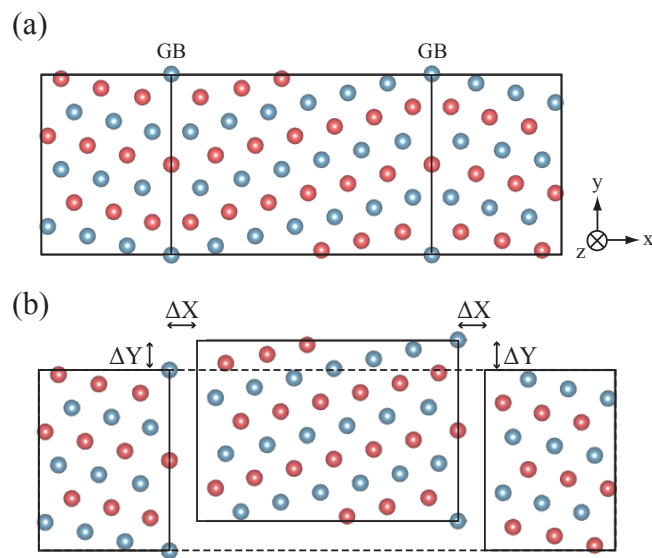


Figure 2: (a) Atomic configuration of the GB supercell of the fcc-Al [110] $\Sigma 9$ symmetric tilt GB. The red and blue balls denote Al atoms in the (110) and (220) atomic layers. (b) One of two grains is rigidly shifted in the two dimension with ΔX and ΔY .

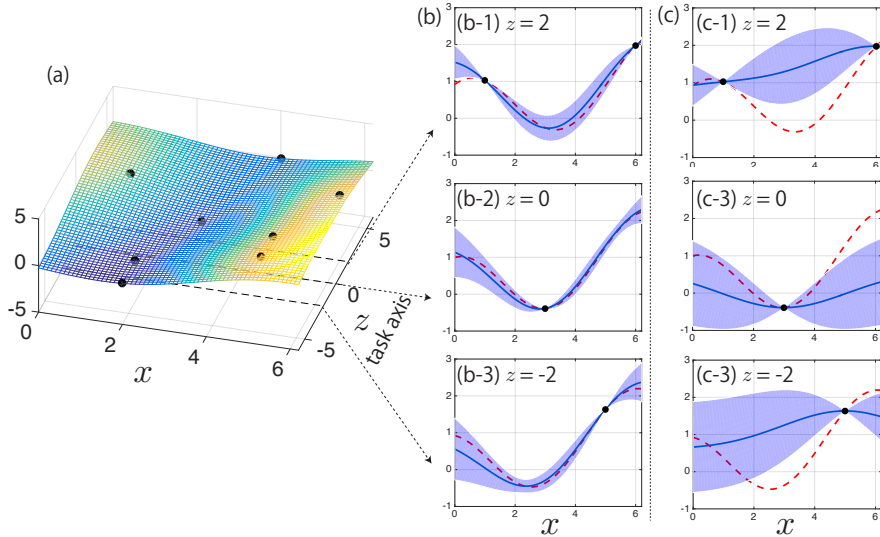


Figure 3: A schematic illustration of MTGP. The left three dimensional plot (a) shows the MTGP mean function surface $\mu^{(\text{MT})}$ in the space of the GB model descriptor \boldsymbol{x} and the task descriptor \boldsymbol{z} (the black points are the sampled data). The center plots (b) show the surfaces for the three different tasks neighboring each other in the task axis. The blue lines are mean functions with the blue shaded standard deviations, and dashed red lines are underlying true functions. Since information of the sampled data is shared, all the mean functions provide good approximations for the true functions compared with the separated estimation of each task illustrated in (c). For example, in $z = -2$ by MTGP (b-3), the smallest points around $x = 2.5$ is accurately approximated by MTGP with sampling only one point which is far from the minimum. This is possible because a point close to the minimum is already sampled in the neighboring task $z = 0$ (b-2). This information is transferred to $z = -2$ with uncertainty determined by the task kernel (task similarity). The minimum of the $z = 2$ (b-1) is also accurately approximated compared with (c) because of the information transfer.

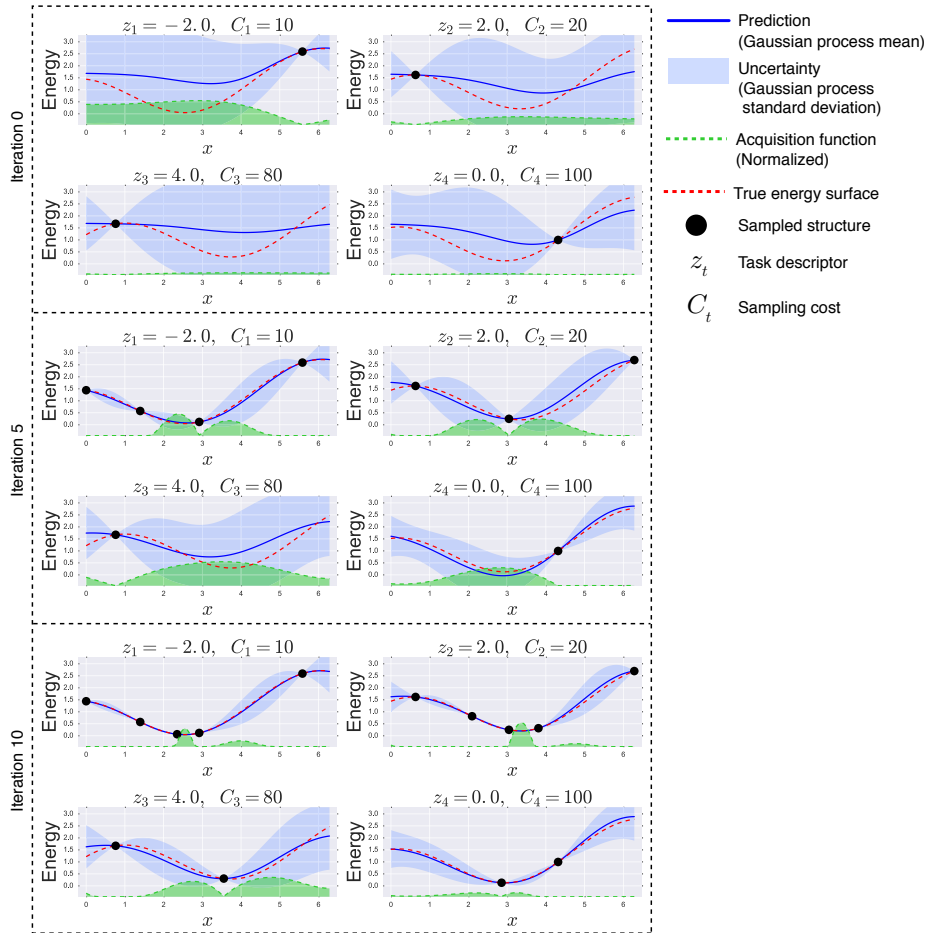


Figure 4: An illustrative example of the proposed method for the synthetic four tasks $t = 1, \dots, 4$ with cost $C_1 = 10$, $C_2 = 20$, $C_3 = 80$, and $C_4 = 100$. In the iteration 0, the initial points are randomly set. Our method first investigates the low cost surfaces $t = 1$ and 2 as indicated by the acquisition function (green lines). In the iteration 5, with the increase of the low cost surface points, uncertainty of the Gaussian process model is reduced even for the high cost surfaces $t = 3$ and 4 in which no additional points are sampled yet. Then, the acquisition function values for the low cost surfaces are decreased because possible improvement is not large any more, and acquisition function values for the high cost surfaces become relatively large. In the iteration 10, the small energy points in the high cost surfaces are identified with the small numbers of samplings.

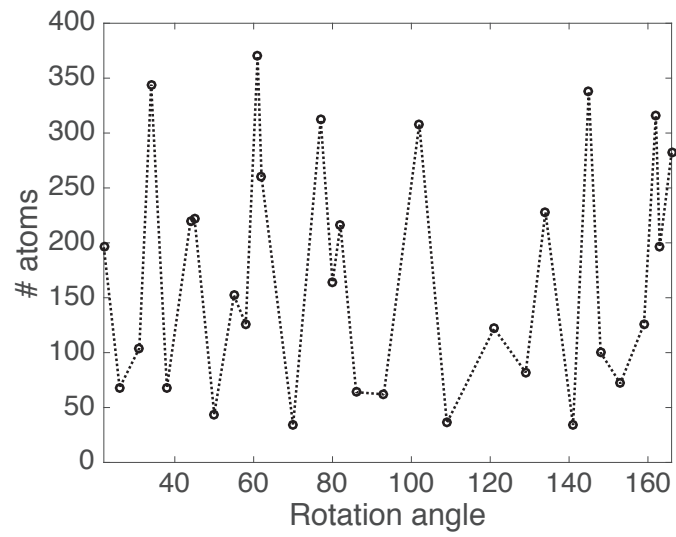


Figure 5: The number of atoms contained in the supercells of the different angles.

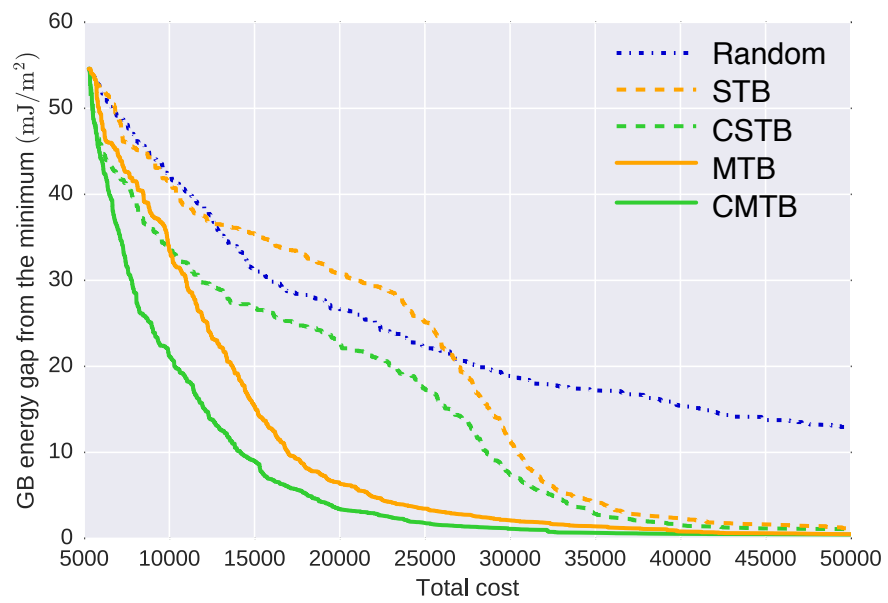
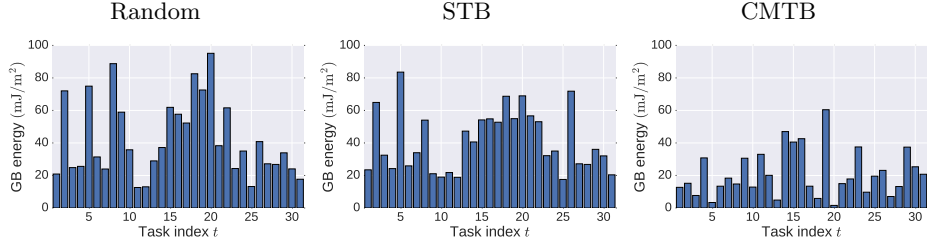
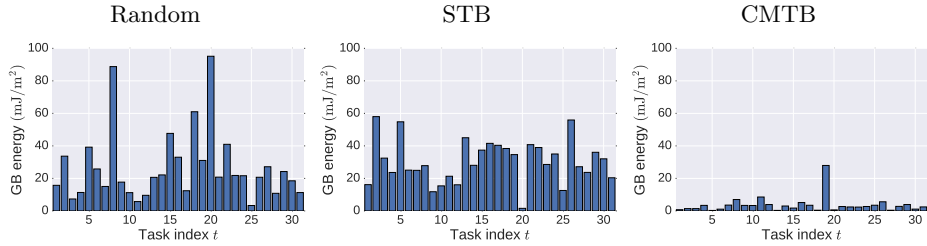


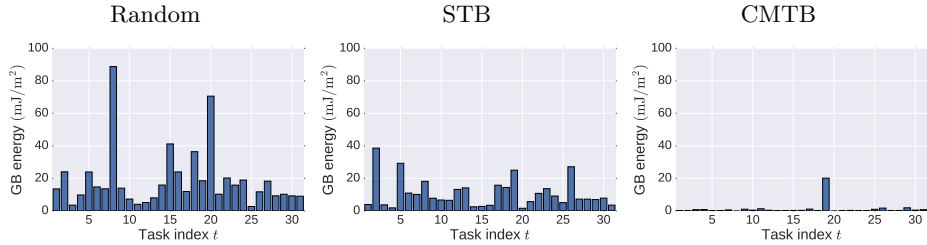
Figure 6: The GB energy gaps from the minimums to the identified structure by each method. The vertical axis is the mean for all angles.



(a) Total cost $C = 10000$

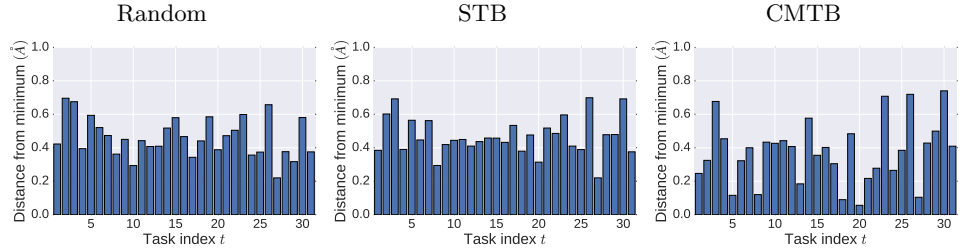


(b) Total cost $C = 20000$

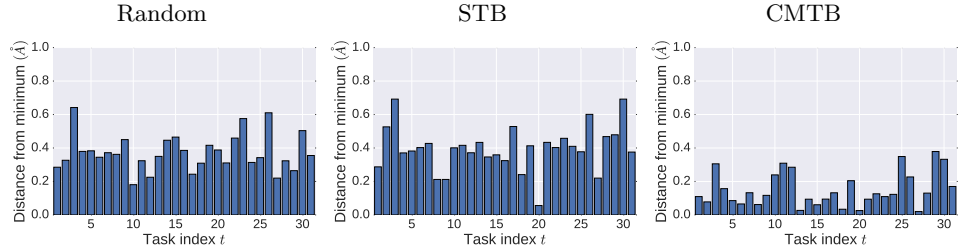


(c) Total cost $C = 30000$

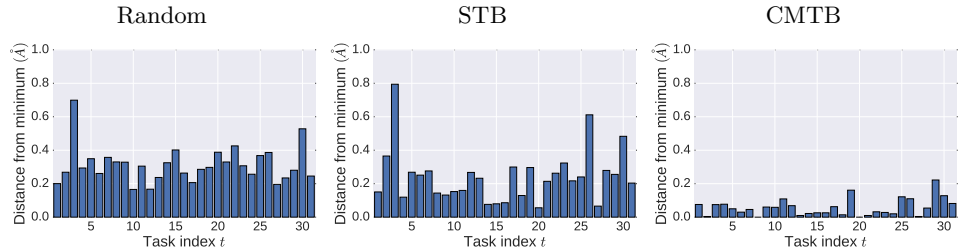
Figure 7: Comparison of the identified GB energies within given total cost values (the average of 10 runs). The vertical axis is separately standardized in such a way that the minimum in each angle becomes zero. The horizontal axis is the task index t .



(a) Total cost $C = 10000$



(b) Total cost $C = 20000$



(c) Total cost $C = 30000$

Figure 8: Comparison of distances in the RBT space (X, Y) from the true minimums to the GB structure having the smallest GB energy in the sampled GB within given total cost values (the average of 10 runs). The horizontal axis is the task index t .

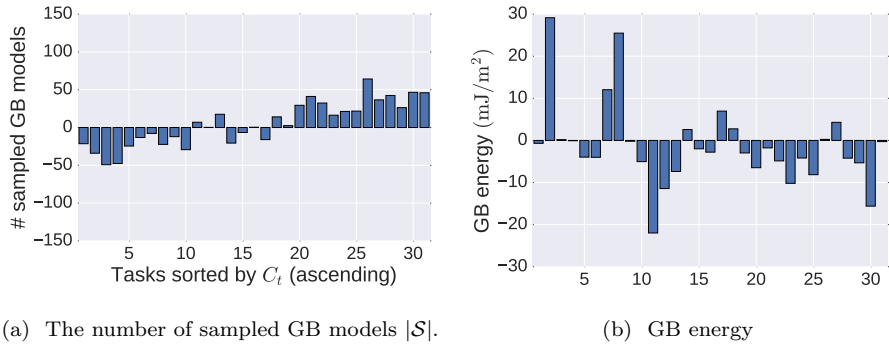


Figure 9: The comparison between MTB and CMTB at the iteration in which 3 GB models are sampled for the task indicated by the horizontal axis (note that here the number of iteration is different for each bar). The vertical axis of the both plots are defined by subtracting results of MTB from CMTB.